



OPEN ACCESS

EDITED BY

Marta Plavsic,
Rudjer Boskovic Institute, Croatia

REVIEWED BY

Sotirios Karavoltzos,
National and Kapodistrian University of
Athens, Greece
Xingwei Meng,
Ministry of Natural Resources, China

*CORRESPONDENCE

Xuefa Shi

✉ xfshi@fio.org.cn

Chuanshun Li

✉ lichuanshun@fio.org.cn

RECEIVED 18 January 2025

ACCEPTED 10 March 2025

PUBLISHED 07 April 2025

CITATION

Li B, Shi X, Li C, Wang S, Ye J, Yan Q, Dang Y
and Fang X (2025) Biogeochemical sulfide
mineralization in the volcanic-hosted
Tongguan hydrothermal field,
southern Mid-Atlantic Ridge.
Front. Mar. Sci. 12:1562763.
doi: 10.3389/fmars.2025.1562763

COPYRIGHT

© 2025 Li, Shi, Li, Wang, Ye, Yan, Dang and
Fang. This is an open-access article distributed
under the terms of the [Creative Commons
Attribution License \(CC BY\)](https://creativecommons.org/licenses/by/4.0/). The use,
distribution or reproduction in other forums
is permitted, provided the original author(s)
and the copyright owner(s) are credited and
that the original publication in this journal is
cited, in accordance with accepted academic
practice. No use, distribution or reproduction
is permitted which does not comply with
these terms.

Biogeochemical sulfide mineralization in the volcanic-hosted Tongguan hydrothermal field, southern Mid-Atlantic Ridge

Bing Li^{1,2,3}, Xuefa Shi^{1,2,3*}, Chuanshun Li^{1,2,3*}, Sai Wang^{1,2,3},
Jun Ye^{1,2,3}, Quanshu Yan^{1,2,3}, Yuan Dang^{1,2,3} and Xisheng Fang^{1,2,3}

¹Key Laboratory of Marine Geology and Metallogeny, First Institute of Oceanography, Ministry of Natural Resources, Qingdao, China, ²Laboratory for Marine Geology, Qingdao Marine Science and Technology Center, Qingdao, China, ³Key Laboratory of Deep Sea Mineral Resources Development, Shandong (Preparatory), Qingdao, China

Biogeochemical mineralization is increasingly recognized as a significant factor in the formation of submarine hydrothermal sulfide deposits. While several mechanisms by which hydrothermal organisms may facilitate metal deposition have been documented in many seafloor hydrothermal deposits, the potential involvement of biogenic processes in the mineralization of hydrothermal deposits in the southern Mid-Atlantic Ridge (SMAR) has been largely overlooked until now. In this study, we investigate sulfide chimney sample from the volcanic-hosted Tongguan hydrothermal field on the SMAR and present several lines of evidence for biogeochemical mineralization. Mineralogical analysis infers four types of biogenic pyrite and chalcopyrite structures: macrobiotic-related tube structures, microbial-related quasi-stromatolite, quasi-oncolite and globular structures. These biogenic structures exhibit selective enrichment of elements such as Mn, Pb, and Cu in biogenic pyrite compared to abiotic pyrite. *In-situ* sulfur isotope studies indicate that biogenic minerals possess lower $\delta^{34}\text{S}$ values than abiotic minerals. We identified three biomineralization mechanisms: an "active" mineralization process mediated by macro-organism, a "passive" mineralization process associated with microbial mats, and a microbial assimilatory sulfate reduction process. Our research suggests that the role of biogenic processes in SMAR hydrothermal mineralization should be given further consideration.

KEYWORDS

biogeochemical mineralization, southern Mid-Atlantic Ridge, sulfide, biogenic structure, mineral chemistry, *in-situ* sulfur isotope

1 Introduction

Modern seafloor hydrothermal systems represent some of the most extreme environments on Earth, capable of supporting oases of life that flourish in high temperatures and perpetual darkness (e.g. Corliss et al., 1979; Humphris et al., 1995). Within these settings, a high diversity of microorganisms, encompassing both Bacteria and Archaea, derives energy from inorganic compounds through a process known as chemosynthesis, colonized on the hydrothermal vents (Corliss et al., 1979; Cavanaugh et al., 1981). Furthermore, numerous microorganisms support macrofaunal communities in a symbiotic relationship, populating the hydrothermal vent ecosystems (Cavanaugh et al., 1981).

Microorganisms associated with mid-ocean ridge vent systems have demonstrated the capacity to thrive within a broad temperature range from 2°C to 122°C (Dick, 2019; Früh-Green et al., 2022). The volcanic-hosted hydrothermal fields, characterized by their relatively high fluid temperatures and an abundance of metals and volatile compounds, support a more diverse microbial community compared to the ultramafic fields influenced by serpentinization, which are predominantly inhabited by methane-metabolizing archaea (Schrenk et al., 2004). In these volcanic environments, a variety of microorganisms thrive, including sulfate-reducing bacteria, sulfide-oxidizing bacteria, methanogens, iron-oxidizing bacteria, and others. This biodiversity underpins an even more varied array of vent fauna, contributing to the complex ecosystem dynamics of these deep-sea habitats (Amend et al., 2011; Früh-Green et al., 2022).

The role of micro- and macro-organisms in seafloor mineralization has been extensively explored in previous studies (Juniper and Fouquet, 1988; Zierenberg and Schiffman, 1990; Koski et al., 1994; Piercey, 2015). Firstly, the metabolic processes of microorganisms themselves involve the reduction of sulfates, which can directly lead to the production of H₂S. This H₂S can then react with iron ions to form framboidal pyrite at the micron scale (Canfield, 2001; Piercey, 2015; Piercey et al., 2018), and such microbial sulfate reduction is considered to play a significant role in the initial stages of seafloor sulfide mineralization (Nozaki et al., 2020). Beyond metabolism, microorganisms can also facilitate sulfide precipitation through “passive” nucleation processes (Jonasson and Walker, 1987; Juniper and Fouquet, 1988). For instance, the bacterial mats near low-temperature hydrothermal vents can provide nucleation surfaces for the precipitation of hydrothermal minerals. Additionally, microorganisms may induce local sulfide precipitation by altering the pH or sulfur fugacity (f_{S_2}) in the microenvironments of bacterial mats (Hannington et al., 1995). Meanwhile, macro-organism can promote sulfide precipitation through “active” mediation (Zierenberg and Schiffman, 1990). For instance, polychaete worms typically secrete mucous layers that can accumulate sulfur and trace elements (such as Cd, Cu), and inherently present in the mucus (Juniper et al., 1986). These mucous layers trap metals and precipitate them as sulfides through adsorption or complexation with soluble species in the organic matrix (Hannington et al., 1995).

These micro- and macro-organisms participate in the mineralization process through various forms, creating specific biogenically formed structures (Cook and Stakes, 1995; Hannington et al., 1995; Piercey, 2015; Nozaki et al., 2020). Mineralogical evidence for this includes the presence of biological structures or their remnants within sulfides (Hannington and Scott, 1988; Juniper et al., 1992; Koski et al., 1994), as well as mineral textures in sulfides that can be explained by microbial activity (Hannington et al., 1995). These phenomena indicate that micro- and macro-organisms play a significant role in the mineralization process of seafloor hydrothermal sulfides.

Compared to other mid-ocean ridges, the investigation and research on hydrothermal sulfides along the Southern Mid-Atlantic Ridge (SMAR) are relatively limited. As an important part of the global mid-ocean ridges, the SMAR is presumed to have a potentially diverse high-temperature hydrothermal fields (Fouquet et al., 2013). It is speculated that, like other hydrothermal fields, there is significant involvement of biomineralization in the hydrothermal mineralization process. However, prior to this, there have been no research reports on biogenic mineralization in the SMAR, and it is unclear whether biology is involved in the mineralization and what types of mineralization occur on SMAR.

In 2015, a hydrothermal field named Tongguan (27.1°S), characterized by the presence of hydrothermal sulfides and biota, was discovered on the SMAR (Wang et al., 2022). This is an active volcanic-hosted high-temperature hydrothermal field where hydrothermal deposits accumulate on the sediment-free basaltic seafloor. The chimney wall fragment was sampled during this expedition. In this study, we identified evidence of Biogeochemical mineralization in terms of mineralogy, mineral chemistry, and *in-situ* sulfur isotopes from the studied sample. The biological entities involved in the hydrothermal mineralization include both micro-organisms and macro-organisms. This further confirms the ubiquity of biogenic mineralization in seafloor hydrothermal systems.

2 Tongguan hydrothermal field

The Tongguan hydrothermal field (27.15°S, 13.45°W; water depth ~3300m) stands as the most southerly discovered hydrothermal field in the SMAR to date. The SMAR is a slow-spreading ridge, and its ridge axis features a prominent central rift valley. The rift valley is defined by a graben-like structure, with an inner valley delineated by a succession of normal bounding faults. The topographical data shows that the ridge exhibits symmetrical spreading, centered on the rift valley, with a series of symmetrical linear volcanic ridges on both flanks of the axis (Figure 1). The active Tongguan hydrothermal field is developed on the newly formed volcanic ridge in the middle of the rift valley, it is a typical sediment-free hydrothermal field.

Through the near-bottom observations by the manned submersible, the Tongguan hydrothermal field is directly developed on fresh pillow basalt (Figure 2a). Active black smoker vents can be seen (Figure 2b), and in their vicinity, numerous

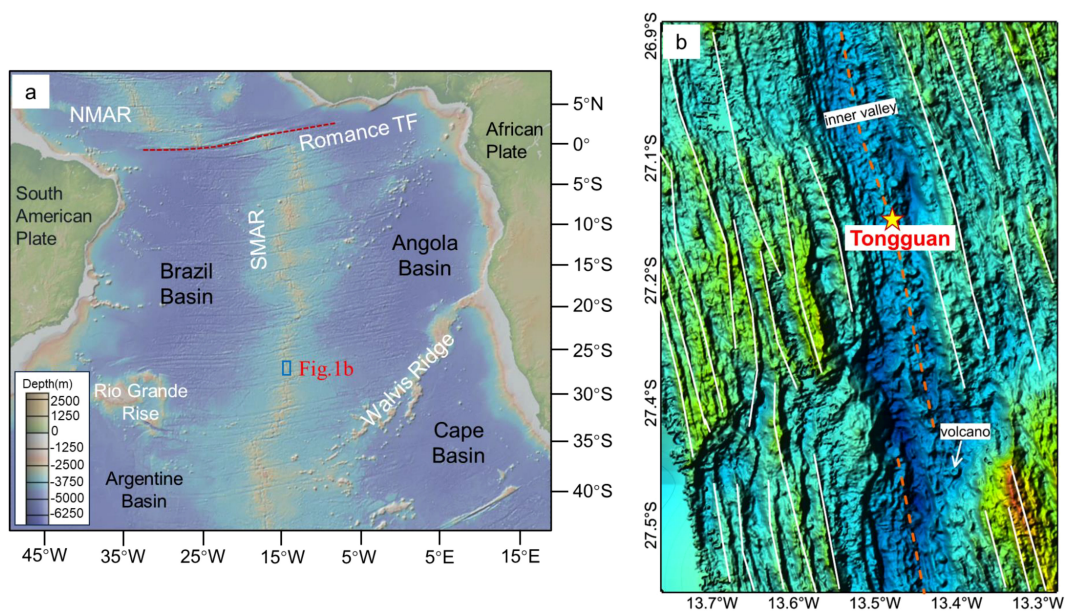


FIGURE 1 Tectonic boundaries and location of **(b)** along the southern Mid-Atlantic Ridge. **(b)** The topographic map of the ridge segment where the Tongguan **(a)** hydrothermal field is located, as measured by the shipborne multibeam survey.

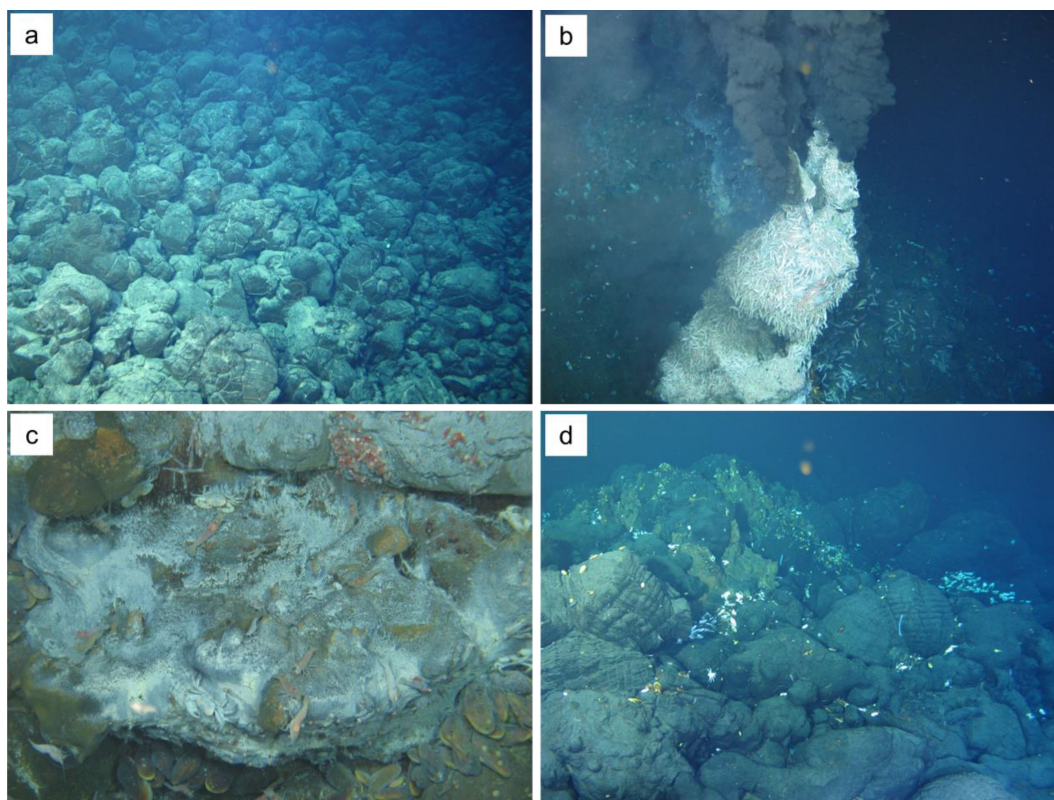


FIGURE 2 Photographs of the Tongguan hydrothermal vent field. **(a)** A large amount of fresh pillow basalt near the vent field. **(b)** An active hydrothermal vent edifice covered with countless hydrothermal blind shrimp. **(c)** White bacterial mats on the surface of sulfide edifices, along with microorganism such as blind shrimp, hydrothermal crabs, and mussels. **(d)** Small-scale inactive chimney structures and hydrothermal biological remains on the pillow basalt.

hydrothermal macro-organisms, mainly blind shrimp, crabs, and mussels, are visible. In addition, on the outer surface of the local hydrothermal edifice without enormous venting, a white bacterial mat can be seen (Figure 2c), which serves as a primary producer, providing a food source for large organisms like blind shrimp. Near the locally deceased chimney structures, a certain amount of biological remains can also be observed (Figure 2d).

3 Sample and methods

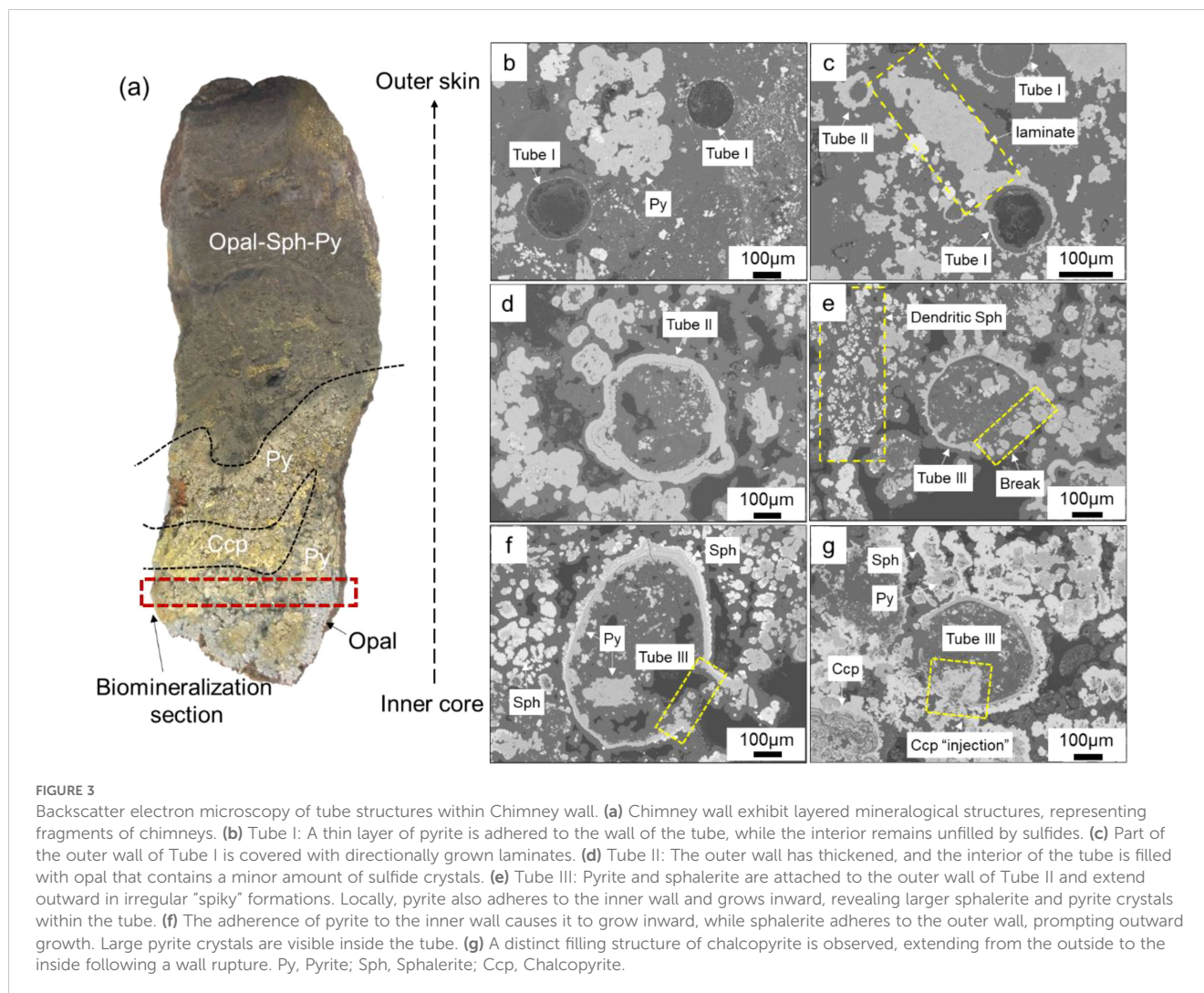
The specimens examined in this research were gathered from the Chinese Ocean 33 expedition conducted in 2015. The collection of all specimens was carried out utilizing a TV grab. During the seaward operations, having pinpointed the site of the hydrothermal sulfide deposit through the use of towed cameras, we deployed a towed TV grab to harvest samples of hydrothermal sulfides.

The studied sample (Figure 3a) shows a fragment of a sulfide chimney wall characterized by mineral banded structures, such as the cross-section of a classic black smoker chimney (Haymon, 1983), exhibiting a sequence of various mineral aggregates that

transition progressively from the interior to the exterior. The innermost layer is composed of coarse-grained chalcopyrite and quartz, while the outer layers are made up of fine-grained pyrite and sphalerite bands. Biogenic structures are primarily concentrated in the inner part.

The sample was first cut and polished into thin sections for further mineralogical and electron probe analysis. Optical reflection microscopy and Back Scattered Electron Imaging (BSE) were utilized in conjunction for the identification of minerals and the interpretation of textures. Microscopic observations were conducted using a Zeiss Axioskop 40 microscope, with magnifications ranging from 100 to 500 times.

For mineral chemical and BSE analysis, a JXA-8230 model Electron Probe X-ray Micro-Analyzer (EPMA) manufactured by JEOL (Japan Electron Optics Laboratory Co., Ltd.) was employed. The operating conditions were set as follows: an incident current of 2.0×10^{-8} A, an acceleration voltage of 15 kV, and a beam spot size of $1.0 \mu\text{m}$. Simultaneous measurements were conducted for elements such as Fe, S, Cu, Zn, As, Pb, Mo, Co, Ni, Mn, Si, and Ag. The mineralogical and EPMA work was conducted at the Key Laboratory of Marine Geology and Metallogeny, FIO.



In-situ sulfur isotope analysis of pyrite and chalcopyrite was performed using the combination of a Teledyne Cetac Technologies Analyte Excite laser-ablation system (Bozeman, Montana, USA) and a Nu Instruments Nu Plasma II MC-ICP-MS (Wrexham, Wales, UK). During the experiment, the energy density of the laser beam used was 2.5 J/cm². Each acquisition included a 30-second background (gas blank) measurement, followed by a spot diameter of 33 μm (for pyrite) and 50 μm (for chalcopyrite) at a repetition rate of 5 Hz for 35 seconds. Helium (800 ml/min) was applied as a carrier gas to efficiently transport the aerosol out of the ablation cell and was mixed with argon (~0.9 L/min) via a T-connector before entering the ICP torch. Natural-pyrite Wenshan ($\delta^{34/32}\text{S} = +1.1\%$ V-CDT) and chalcopyrite GBW07268 ($\delta^{34/32}\text{S} = -0.1\%$, from the National Research Center for Geoanalysis, China) were used as external bracketing standards every fourth analysis. Fine-grained-sphalerite NBS 123 ($\delta^{34/32}\text{S} = +17.1\%$, from the National Institute of Standards and Technology, U.S.) and chalcopyrite TC1725 ($\delta^{34/32}\text{S} = +12.8\%$) were treated as quality controls. The long-term reproducibility of $\delta^{34}\text{S}$ is better than 0.5‰ (1 Standard Deviation). The work was completed at Nanjing FocuMS Technology Co. Ltd.

4 Results

4.1 Biogenic mineralogy

Biogenic structures often exhibit regularly shaped, anhedral mineral aggregates. Based on the mineral and aggregate patterns, we suggest that there are four types of potential biogenic structures (Table 1): tube structure, quasi-oncolite structure, quasi-stromatolite structure and globular structure. These structures are confined to specific section in the core part of the wall.

4.1.1 Tube structure

A certain amount of tube structure has been identified in chimney wall, which developed in the opal matrix. Within chimney wall, tube structures are associated with the quasi-

oncolite and quasi-stromatolite structures (see the text below), with a distribution width of several hundred micrometers.

Based on the mineral filling and wall rupture of the tubes, tube structures can be categorized into three types. Tube I is characterized by a thin-walled tube composed of iron sulfides, which is hollow inside or filled with opal but not with sulfides (Figures 3b, c). Some Tube I structures have locally thickened walls due to the attachment of outward-growing pyrite laminates (Figure 3c). Tube II is an extension of Tube I where the wall is further thickened by the attachment of sulfide minerals and partially filled with a small number of sulfide aggregates (Figure 3d). Tube III, building on Tube II, shows further growth of the tube wall either inward or outward, with a noticeable presence of large sulfide aggregates inside (~100 μm, Figures 3f, g). In some cases, it is clearly visible that chalcopyrite fills the tube from the outside in following wall rupture (Figure 3g).

4.1.2 Quasi-oncolite structure

Within the chimney wall, several quasi-oncolite structures was identified, exhibiting a close symbiotic relationship with tube structures. These quasi-oncolites bear a striking resemblance to oncolites found in carbonate rocks (Weiss, 1969), thus we refer to it as a quasi-oncolite structure. They are characterized by a sequence of bands that envelop an initial nucleus (Figure 4), facilitating a laminate growth pattern resembling microbially induced layered microbial rocks (Grotzinger and Al-Rawahi, 2014). The assemblage includes quasi-oncolites predominantly composed of pyrite (Figures 4a, b) as well as structures where chalcopyrite is the primary component (Figures 4c, d). At the heart of these quasi-oncolite structures lies a nucleus, which may consist of early-stage pyrite crystals (Figure 4a) or opal (Figures 4b–d). This nucleus is encased in a shell of irregular, concentrically banded layers, which alternate between light and dark layers. The light layers are chiefly composed of colloform sulfide minerals, whereas the dark layers are predominantly composed of amorphous silica with impurities. The resultant quasi-oncolite structures are notably large, with some reaching a maximum size more than 300 μm.

TABLE 1 Characteristics of the four biogenic structures in the Tongguan hydrothermal field.

Biogenic Structure	Description	Associated Features
Tube Structure	<ul style="list-style-type: none"> - Thin-walled tube of iron sulfides - Hollow or filled with opal and sulfides - Locally adhered with pyrite laminates 	<ul style="list-style-type: none"> - Between granular chalcopyrite and pyrite zones - Associated with quasi-oncolite and quasi-stromatolite structures
Quasi-oncolite Structure	<ul style="list-style-type: none"> - Bands enveloping an initial nucleus - Composed predominantly of pyrite or chalcopyrite - Nucleus of early-stage pyrite or opal crystals - Laminate contains Light and dark layers 	<ul style="list-style-type: none"> - Close symbiotic relationship with tube structures - Similar to oncolites
Quasi-stromatolite Structure	<ul style="list-style-type: none"> - Grows along a dominant direction on an early basement - Laminate contains Light and dark layers - Basements of early-stage pyrite and chalcopyrite aggregates 	<ul style="list-style-type: none"> - Close symbiotic relationship with tube structures - Similar to stromatolites
Globular Pyrite	<ul style="list-style-type: none"> - Single globular or aggregates - Diameters from 10 to 40 μm - Some appear "dirty" due to impurities - Nucleus for growth of other mineral aggregates 	<ul style="list-style-type: none"> - Can adhere to the outer wall of tubes

4.1.3 Quasi-stromatolite structure

The quasi-stromatolite structure located within chimney wall exhibit a laminate like that of the quasi-oncolite structure, which is composed of alternating light and dark layers (Figure 5). The difference lies in the fact that the quasi-stromatolite structures develop on an early “basement”, growing along a pronounced dominant direction with varying heights of several tens of micrometers, rather than growing in concentric bands around a nucleus like the quasi-oncolite structure. This resembles the stromatolites associated with algal growth (Hohl and Viehmann, 2021), thus we refer to it as a quasi-stromatolite structure. The laminates are not closed. The “basement” colonized by the laminates consist of early-stage pyrite and chalcopyrite aggregates, or an early quasi-oncolite. The mineral composition of the laminates is the same as that of the quasi-oncolite structure.

4.1.4 Globular structure

Based on the occurrence patterns, the globular pyrite can be classified into three types: (1) single globular, with diameters ranging from 10 to 40 μm (Figures 6a–d), some of which appear relatively “dirty” due to the presence of impurities (Figures 6a–c); (2) serving as the nucleus for the growth of other mineral aggregates (Figures 6a, b), where later-stage colloform pyrite can grow in concentric bands around the early globular pyrite, forming central

bands. Under the action of surface energy, multiple pyrite aggregates, each having globular pyrite at its nucleus, can combine to form larger aggregates (Sawlowicz, 1993). (Figure 6a). The later-stage colloform pyrite can also grow along a dominant direction to form a laminate (Figure 6b). Additionally, globular pyrite can be directly enveloped by later-stage sphalerite (Figure 6a); (3) globular pyrite aggregates (Figures 6c, d), formed by the direct aggregation of multiple globular pyrites (Figures 6c, d); locally, single globular pyrite can also adhere directly to the outer wall of the tubes (Figure 6d).

4.2 Mineral chemistry

The chemical compositions of biogenic pyrite and chalcopyrite, as well as the compositions of abiotic pyrite and chalcopyrite that developed adjacent to those biogenic minerals, as determined by EPMA, are presented in Supplementary Tables 1–6. Their statistical values are summarized in Table 2.

By comparing the four types of biogenic pyrite with abiotic pyrite, several significant differences in mineral element composition can be observed (Table 2; Figure 7): compared to the abiotic pyrite, which has a more concentrated content of Fe (46–48 wt%) and S (52–54 wt%), the major elements Fe and S in the four

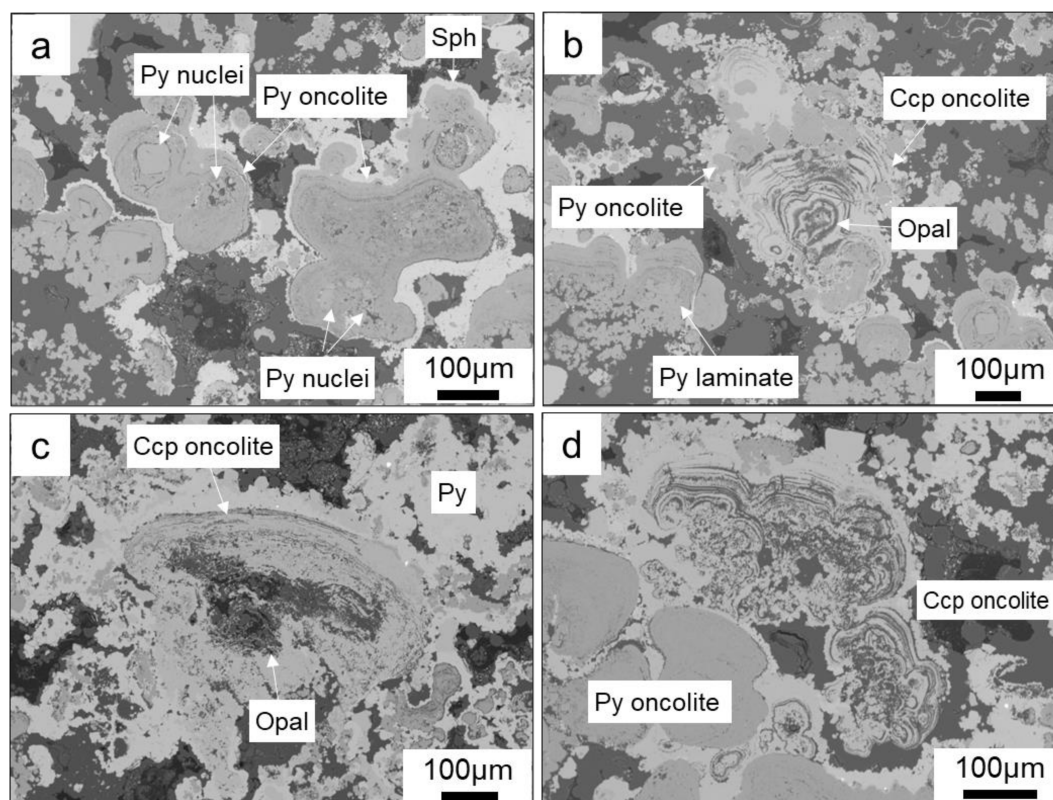


FIGURE 4

Backscatter electron microscopy of Quasi-oncolite structures within chimney wall. (a) Quasi-oncolite Structures with early pyrite crystals as the nuclei, generally formed by the fusion of multiple-nuclei closed pyrite laminates; (b–d). Quasi-oncolite structures with nuclei primarily composed of crystals containing amorphous silica. In (b), the chalcopyrite laminates encase a certain amount of small pyrite-dominated oncolites, while in (c, d), the closed laminates are more irregular in shape, and the oncolites are coated by later-stage pyrite.

types of biogenic pyrite are all lower, and the content of Fe and S has a greater range of variation (Figure 7a). Although the major element contents are low, the trace element contents of Mn (with an average value ranging between 0.17-0.35 wt%) and Pb (with an average value ranging between 0.35-0.74 wt%) in the four types of biogenic pyrite are all higher than those in abiotic pyrite (Mn average 0.03 wt%, Pb average 0.17 wt%), and they have a larger range of variation, whereas the trace element variation range in abiotic pyrite is smaller (Figures 7b, c).

The difference in Mo content between biogenic and abiotic pyrites is not significant (Figure 7d), mostly ranging between 0.9-1.1 wt%. The average Mo content in biogenic pyrite increases, which is related to inclusions reaching up to 4 wt% locally (Supplementary Table 2). In addition, although the Zn content in biogenic pyrite is also higher than that in abiotic pyrite, this increase is related to the replacement of biogenic pyrite by later sphalerite (Figures 3f, 5a, 6a, b). Moreover, except for globular pyrite, the Cu content in other biogenic pyrites is also significantly higher than that in abiotic pyrite.

Compared to abiotic chalcocopyrite, the two types of biogenic chalcocopyrite (quasi-stromatolite and quasi-oncolite chalcocopyrite) both have relatively slightly lower contents of Fe, Cu, and S (Table 2), and they exhibit a relatively larger range of variation (Figures 8a, b). In terms of trace elements, individual biogenic chalcocopyrite crystals have higher Zn contents due to the presence of

sphalerite inclusions (Supplementary Tables 2&3), while the rest of the biogenic chalcocopyrite crystals and abiotic chalcocopyrite do not contain Zn. Additionally, except for the quasi-stromatolite chalcocopyrite, which has a relatively slightly higher Pb content (Figure 8c), there are no significant differences in other trace elements.

4.3 *In-situ* sulfur isotope

A total of 37 *in-situ* sulfur isotopes were conducted on sulfide minerals, including 29 samples of biogenic/abiotic pyrite, as well as 8 samples of biogenic/abiotic chalcocopyrite. The results are presented in Table 3 and illustrated in Figure 9. For the biogenic minerals, the $\delta^{34}\text{S}$ values of 3 pyrite spots on the tube wall range from 2.8-4.1‰, those of 4 pyrite spots from the laminate of the quasi-oncolite structure range from 2.0-3.5‰, and the $\delta^{34}\text{S}$ values of 2 pyrite spots from the laminate of the quasi-stromatolite structure are 3.4‰ and 3.7‰, respectively. Additionally, the $\delta^{34}\text{S}$ values of 13 globular pyrite spots range from 1.3-2.8‰, and those of 6 chalcocopyrite spots from the Quasi-oncolite structure range from 2.6-3.6‰. For the abiotic minerals, the $\delta^{34}\text{S}$ values of 7 granular pyrite spots range from 4.0-5.3‰, and both granular chalcocopyrite spots have a $\delta^{34}\text{S}$ value of 4.2‰.

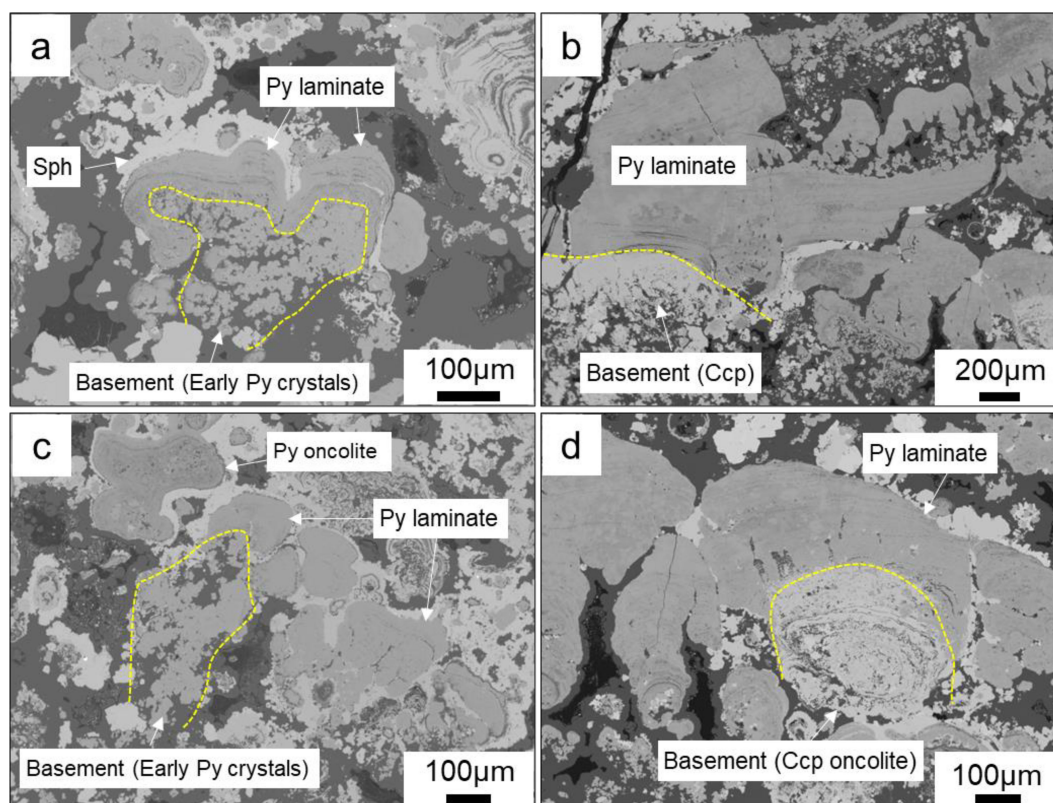


FIGURE 5

Backscatter electron microscopy of quasi-stromatolite structures within Chimney Wall. (a) Pyrite laminate growing on the basement of early subhedral pyrite aggregates, subsequently coated by colloform sphalerite; (b) Pyrite laminate stratifying growth on the basement of early anhedral chalcocopyrite; (c) Pyrite laminate associated with pyrite oncolite; (d) Pyrite laminate growing on the basement of early chalcocopyrite oncolite.

5 Discussion

5.1 Macrobial sulfide mineralization

The tube structures developed in the chimney wall are regarded as biogenic structures related to the activities of macro-organisms in hydrothermal fields, specifically *annelida*, including vestimentiferans, annelid worms, and polychaete worms (Juniper et al., 1986; Cook and Stakes, 1995), reflecting the participation of macro-organisms in the mineralization process. The presence of tube structures in different ridge hydrothermal sulfide deposits and ancient Volcanic Hosted Massive Sulfide (VHMS) has been commonly reported previously (e.g., Hannington and Scott, 1988; Cook and Stakes, 1995; Little et al., 1997; Georgieva et al., 2018).

Annelida are widely found in various seafloor hydrothermal systems (Black et al., 1998; Pedersen et al., 2010; Bright et al., 2024) and their presence is closely associated with chemosynthetic bacteria in hydrothermal fields as primary producers (Georgieva et al., 2018). *Annelida* form external coatings by secreting mucus layers, which passively adsorb and capture metal ions, precipitating on the outer wall to form metal layers, representing an important type of microbial biomineralization (Hannington et al., 1995; Park and Damien, 2021). Mineralogical chemical analysis shows that the pyrite in the tube walls of this field has significantly higher Mn, Pb

and Cu contents than abiotic pyrite, indicating that the pyrite precipitated during the microbial biomineralization process selectively enriches elements.

Cook and Stakes (1995) proposed the petrological evolution of tube structures, which is divided into five different sequences, starting with low-temperature minerals (such as barite) and gradually transitioning to high-temperature minerals (such as chalcopyrite), representing the evolutionary process of the tube structures. The three evolutionary sequences of tubular structures identified in the Tongguan field (Tube I to Tube III) are consistent with the evolution proposed by Cook and Stakes (1995), which is from an initial low-temperature mineral stage to a subsequent thickening of the tube walls inward and outward, and gradual replacement by high-temperature minerals and the filling of the tube lumen with high-temperature phases. However, according to the evolutionary sequence of Cook and Stakes (1995), with further infilling and recrystallization, the tubes will eventually lose all or most of their layers. But in this field, such structures have not been observed. This indicates that the evolution of the tube structures in this field is incomplete, suggesting that the high-temperature stage in the later period of tube structure evolution was relatively short-lived. Instead, most tube structures in this field are eventually filled with abiotic low-temperature opal precipitates. Additionally, there are laminate structures locally adhering to the tube wall in Tube I

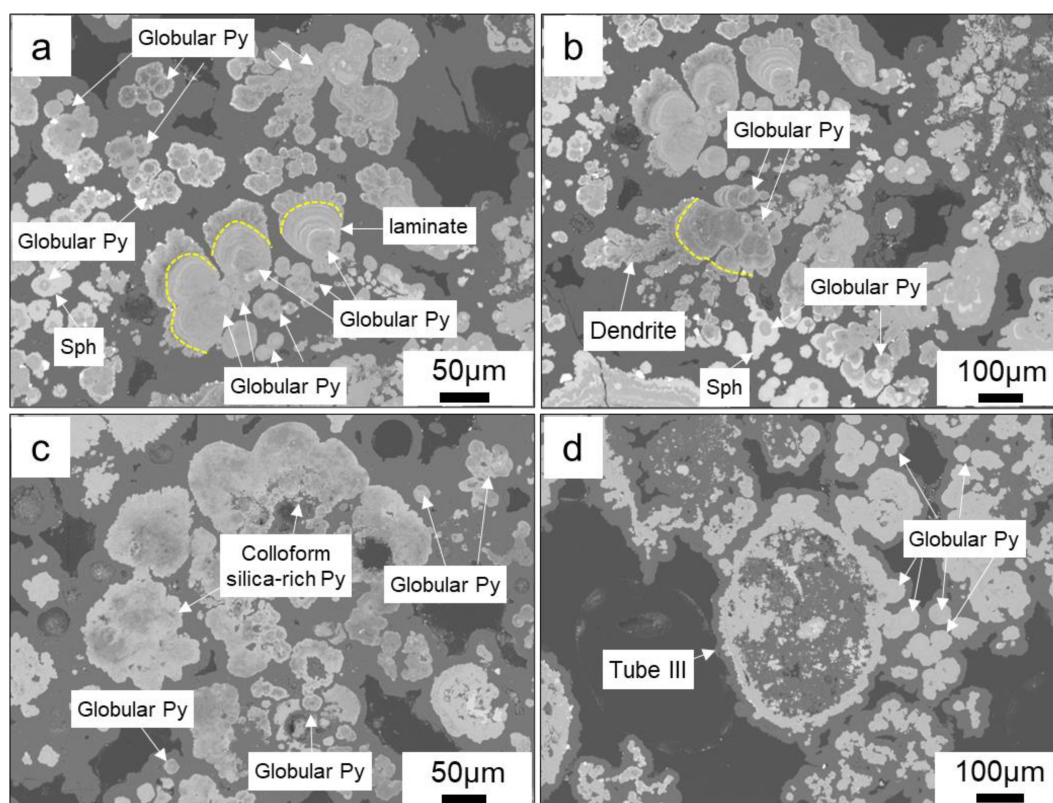


FIGURE 6

Backscatter electron microscopy of globular pyrites. (a, b) Globular pyrite acts as a nucleus for the subsequent growth of minerals, including pyrite laminate, aggregates of globular pyrite, and colloform sphalerite; (c) Individual globular pyrite and its aggregates, associated with colloform silica-rich pyrite; (d) Multiple larger globular pyrites (~30-40µm) form aggregates, and several globular pyrites can be seen adhering to the outer wall of Tube III.

(Figure 6b). The laminate structure is closely associated with the activities of microbes, indicating the coexistence of annelids and microorganisms. In addition, the conditions during the early stage of tube mineralization were also conducive to microbial activity.

5.2 Microbial sulfide mineralization

Bacteria and archaea are an essential part of modern hydrothermal vent communities and are the primary producers in these ecosystems, with their biomass far exceeding that of macroorganisms (Reysenbach et al., 2000; Sievert and Vetriani, 2012). In this field, the outer wall of the hydrothermal vent structure shows development of bacterial mats (Figure 2c). These microorganisms can participate in the hydrothermal mineralization process through various mechanisms (Zierenberg and Schiffman, 1990; Georgieva

et al., 2018; Park and Damien, 2021). Unlike microbial mineralization, which preserves the remains of individual organisms, microbial mineralization exhibits more complex structures. Similar to microbial rocks such as stromatolites and oncolites in sedimentary rocks (Reid et al., 2000; Grotzinger and Al-Rawahi, 2014; Nutman et al., 2016), as well as seabed biogenic polymetallic nodules and ferromanganese crusts with similar structural features (e.g. Wang and Müller, 2009; Zhao et al., 2014; Jiang et al., 2017), we propose that the quasi-stromatolite and quasi-oncolite structures in this field are of microbial origin. However, their formation mechanisms differ.

5.2.1 Laminate pyrite/chalcopyrite

Comparing the quasi-stromatolite and quasi-oncolite structures, apart from the difference between one having a “basement” and the other having a nucleus, they are highly

TABLE 2 Chemical compositions of four types of biogenic pyrite, 2 types of biogenic chalcopyrite, and abiotic pyrite and chalcopyrite as determined by EPMA analysis.

	N		Si	As	S	Ag	Mn	Co	Cu	Ni	Fe	Zn	Mo	Pb
Tu. Py	30	Min	nd	nd	49.96	nd	0.01	0.02	0.17	nd	40.62	0.05	0.93	0.13
		Max	0.65	nd	53.55	0.08	0.49	0.17	0.86	0.07	46.87	7.02	1.09	1.98
		Mean	0.07	nd	51.96	0.03	0.19	0.09	0.42	0.02	44.61	1.02	1.02	0.56
Str. Py	23	Min	nd	nd	47.91	nd	0.04	nd	0.12	nd	44.04	nd	nd	nd
		Max	0.62	nd	52.10	0.06	0.52	0.15	3.95	0.08	46.54	1.50	3.75	0.62
		Mean	0.13	nd	50.43	0.02	0.24	0.07	0.56	0.03	45.59	0.23	1.11	0.35
Str. Ccp	9	Min	nd	nd	33.00	nd	nd	nd	33.13	nd	29.44	nd	0.58	0.11
		Max	0.52	nd	35.64	0.08	0.02	0.12	34.58	0.06	30.88	nd	0.79	0.41
		Mean	0.09	nd	33.91	0.04	0.01	0.05	33.75	0.02	30.19	nd	0.69	0.21
Onc. Py	7	Min	nd	nd	49.28	nd	0.13	0.05	0.18	nd	44.00	0.24	0.95	0.29
		Max	0.57	nd	52.93	0.07	0.67	0.13	0.93	0.08	45.74	1.68	1.05	2.53
		Mean	0.16	nd	51.25	0.02	0.35	0.09	0.41	0.01	44.84	0.95	1.00	0.74
Onc. Ccp	8	Min	nd	nd	33.94	nd	nd	0.02	33.17	nd	28.63	nd	nd	nd
		Max	0.64	nd	35.05	0.11	0.03	0.07	35.69	0.08	30.87	nd	0.79	0.21
		Mean	0.14	nd	34.39	0.04	0.01	0.05	34.28	0.01	29.76	nd	0.28	0.06
Gl. Py	8	Min	nd	nd	50.49	nd	0.09	0.01	nd	nd	44.54	0.10	nd	0.01
		Max	0.75	nd	54.21	0.02	0.29	0.16	0.50	0.06	46.34	0.95	1.06	1.51
		Mean	0.11	nd	52.68	nd	0.17	0.07	0.08	0.02	45.22	0.27	0.84	0.63
Ab. Py	35	Min	nd	nd	49.76	nd	nd	0.01	nd	nd	45.21	nd	nd	nd
		Max	0.34	nd	53.98	0.04	0.13	0.15	2.05	0.08	47.57	0.58	1.13	0.80
		Mean	0.02	nd	52.81	0.01	0.03	0.09	0.31	0.01	46.71	0.15	0.82	0.17
Ab. Ccp	20	Min	nd	nd	33.09	nd	nd	nd	34.09	nd	29.31	nd	nd	nd
		Max	0.32	nd	35.05	0.09	0.04	0.14	35.16	0.05	31.19	nd	0.83	0.28
		Mean	0.02	nd	34.53	0.02	0.01	0.06	34.66	0.01	30.54	nd	0.47	0.09

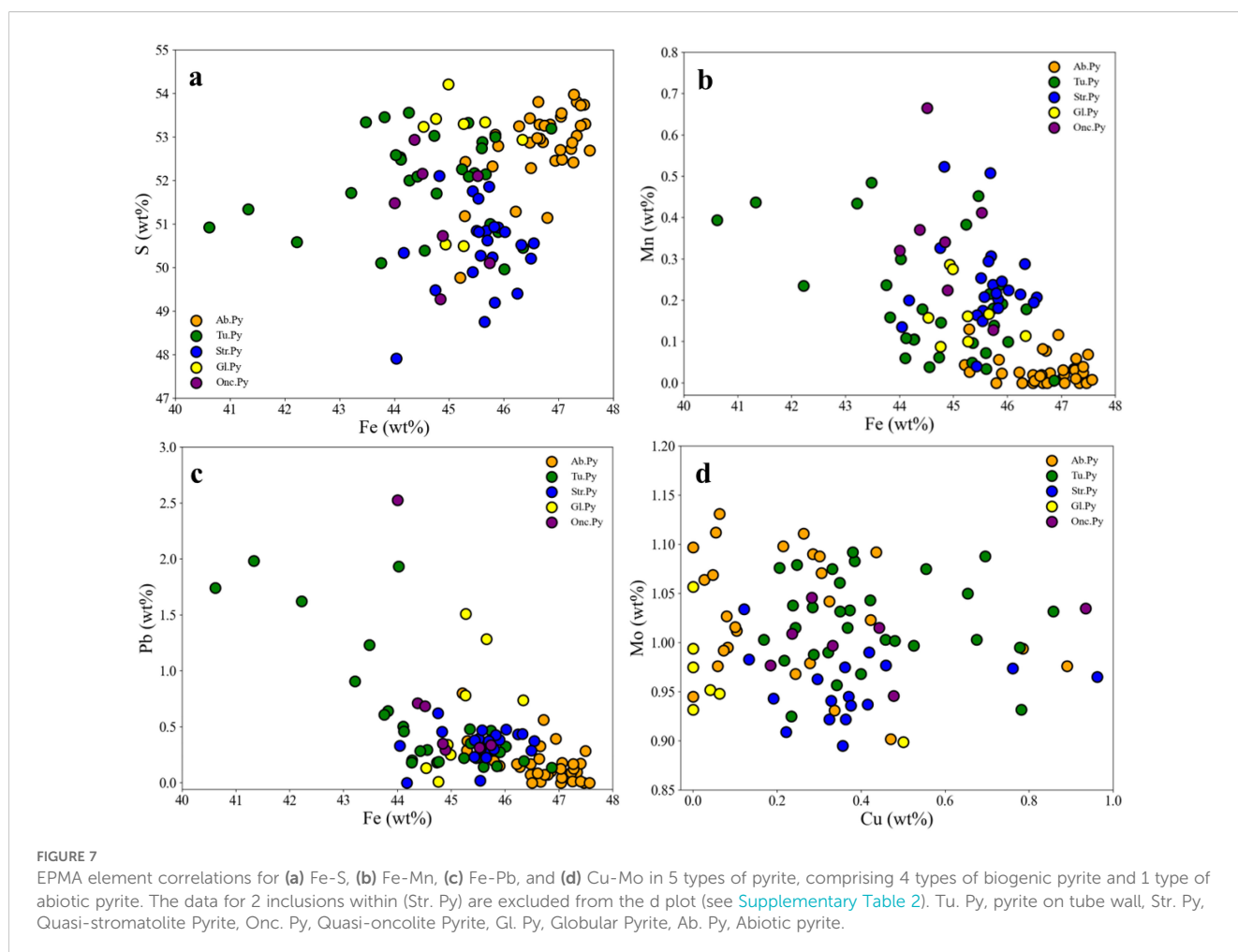
Tu. Py, pyrite on tube wall, Str. Py, Quasi-stromatolite Pyrite, Str. Ccp, Quasi-stromatolite Chalcopyrite, Onc. Py, Quasi-oncolite Pyrite, Onc. Ccp, Quasi-oncolite Chalcopyrite, Gl. Py, Globular Pyrite, Ab. Py, Abiotic pyrite, Ab. Ccp, Abiotic chalcopyrite. N, Number of points. The statistical data excludes several inclusion data points (see Supplementary Tables 2 and 3 for the raw data). nd, non detected. See "Appendix A" for the detailed data.

similar in terms of mineral type and composition: both exhibit laminate structures composed of light and dark layers, with the thickness of individual laminae being essentially uniform. Additionally, the pyrite composition that forms the laminate and their $\delta^{34}\text{S}$ values are also quite similar. The morphological characteristics of this laminate are strikingly like those found in carbonate stromatolites, oncolites and seabed ferromanganese crusts (e.g. Reid et al., 2000; Jiang et al., 2017).

For stromatolites and oncolites, the laminate is formed through the growth and metabolic activities of microbial mats, with the secretion of metabolic by-products by microbial communities inducing mineral precipitation, which is a type of microbially-induced mechanism (Park and Damien, 2021). In seafloor hydrothermal fields, especially those involving low-temperature diffuse fluids, extensive biofilm-forming bacterial mats composed of single-celled and filamentous bacteria are developed, utilizing dissolved reduced minerals (primarily sulfur compounds) or solid metal sulfide deposits emitted from the vents as their chemoautotrophic electron or energy source (Corliss et al., 1979). The bacterial mat resembles the microbial mat that grows in stromatolites, and the mineral precipitation induced by bacterial mats has also been reported in other hydrothermal fields (Corliss et al., 1979; Zierenberg and Schiffman, 1990).

From a mineral chemistry perspective, the laminate pyrite in this field is enriched in Mn, Pb, and Cu (Table 2 and Figure 7). Generally, when abiotic pyrite is enriched in Mn and Pb, it typically indicates a moderate to low-temperature, weakly reducing, or even slightly oxidizing environment. Conversely, when abiotic pyrite is enriched in Cu, it indicates a slightly higher temperature reducing environment (Maslennikov et al., 2009; Keith et al., 2016). The simultaneous enrichment of Mn, Pb, and Cu in pyrite is difficult to explain from an abiotic origin. Furthermore, other granular pyrite crystals in the same analyzed sample location, which share the same physicochemical conditions for precipitation as the laminate, do not enrich in Mn, Pb, and Cu, suggesting that the enrichment of trace elements in the laminate pyrite is not temperature-dependent. We suggest this is due to a bacterial mat-mediated process that selectively precipitates specific metals, as previous studies have shown that bacterial mats in certain hydrothermal fields can selectively enrich in Cu (Zierenberg and Schiffman, 1990).

Both the stromatolite-like and oncolite-like structures are rarely reported in previous studies of seafloor hydrothermal sulfides. From a mineralogical perspective, both structures coexist with the macrobial structure-tube structure in specific part of the chimney wall, indicating similar survival environments. Bacterial mats are likely to provide a food source for *Annelida* (Georgieva et al., 2018).



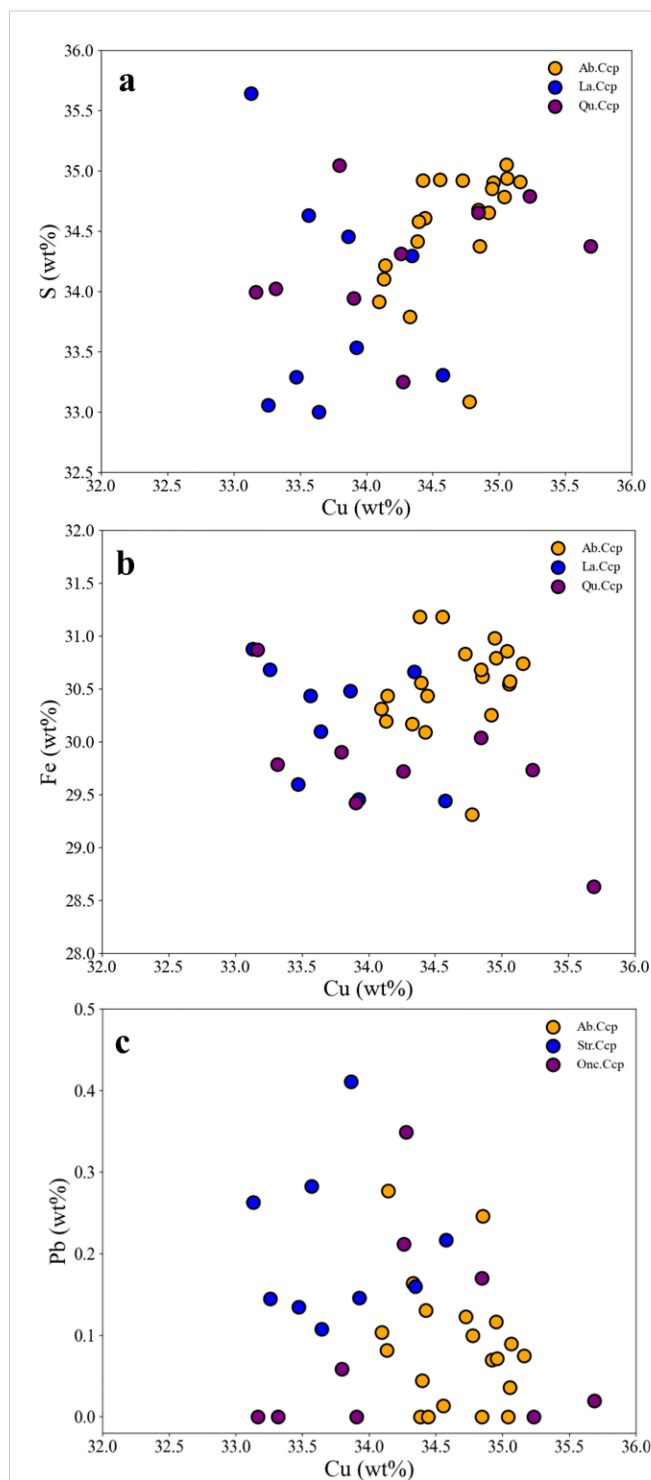


FIGURE 8
EPMA element correlations for Cu-S, Cu-Fe, Cu-Pb in 3 types of chalcopyrite, comprising 2 types of biogenic chalcopyrite and 1 type of abiotic chalcopyrite. In biogenic chalcopyrite, data for several inclusions containing sphalerite are excluded. Str. Ccp, Quasi-stromatolite Chalcopyrite, Onc. Ccp, Quasi-oncolite Chalcopyrite, Ab. Ccp, Abiotic Chalcopyrite.

The presence of a certain amount of laminate adhering to some tubes suggests that there is still bacterial mat activity on the already mineralized tube I, further indicating that the bacterial mats in this area have more extensive survival conditions than *Annelida*.

5.2.2 Globular pyrite

Despite the observation of abiotic globular pyrite formation under certain experimental conditions (Ohfuji and Rickard, 2005; Duverger et al., 2021), the prevailing view is still that globular pyrite under natural conditions is primarily associated with microbial activity (Piercey, 2015; Wacey et al., 2015; Nozaki et al., 2020; Truong et al., 2024). The evidence supporting a biogenic origin includes the selective enrichment of certain elements in pyrite, the presence of a certain amount of organic matter, possible microbial fossils and so on.

In this study, globular pyrite exhibits a relatively “dirty” characteristic (Figure 6), indicating the presence of organic matter. Given that organic matter is necessarily a product of either microbial metabolism or the microbial itself, the association of globular pyrite with organic matter strongly suggests a biogenic origin. As discussed by Duverger et al. (2021), the formation of globular pyrite is closely linked to the presence of organic matter. Biogenic globular pyrite biofilms contain a wealth of organic compounds that may facilitate the formation of these pyrite aggregates. This is reminiscent of framboidal pyrite, which is also biogenic but forms through the aggregation of numerous small pyrite crystals (Sawlowicz, 1993). In comparison to abiotic pyrite, globular pyrite is enriched in Mn and Pb, but not Cu relative to laminar pyrite, suggesting a selective enrichment of certain elements. However, this selective enrichment does not entirely correspond to that observed in bacterial mats within laminar pyrite.

Unlike framboidal pyrite, globular pyrite does not exhibit highly negative $\delta^{34}\text{S}$ values (Sim et al., 2011; Nozaki et al., 2020, down to $\sim -60\%$), but rather has slightly lower $\delta^{34}\text{S}$ values compared to other biogenic pyrite types and a smaller sulfur isotope fractionation of $\sim 4\%$ compared to abiotic pyrite. This indicates that the pyrite biofilm in globular pyrite has not undergone significant microbial sulfate reduction. According to Canfield (2001), lower sulfur isotope fractionation generally corresponds to assimilatory sulfate reduction, where microorganisms convert seawater sulfate (SO_4^{2-}) into sulfide (S^{2-}) and incorporate it into cellular organic sulfur compounds. In this process, because the sulfate transport is unidirectional, no significant sulfur isotope fractionation is observed. Therefore, we believe that the microbial metabolic process related to assimilatory sulfate reduction is the key factor leading to the formation of globular pyrite in this field.

5.3 Models

For decades, biological activities have been considered to play a non-negligible role in the formation of submarine hydrothermal

sulfide deposits (Juniper and Fouquet, 1988; Hannington et al., 1995; Piercey, 2015; Nozaki et al., 2020). Our research further confirms this perspective. However, biogenic minerals are confined to specific locations within chimney structure, rather than throughout the entire sample, indicating that biological activities are subject to strict environmental constraints. From the perspective of mineral paragenesis (Figures 3–6), the laminate structure exhibits characteristics of coexistence with both the tube and globular structures, and the globular structure also shows coexistence with the Tube structure. The bacterial mats associated with the laminate generally require low-temperature hydrothermal conditions (Winn et al., 1986; Zierenberg and Schiffman, 1990), indicating that microbial mineralization in this area primarily occurs at low temperatures.

In this study, three mechanisms by which hydrothermal organisms may facilitate mineral precipitation have been identified (Figure 10). For the Tube structure, as previously revealed by research (Cook and Stakes, 1995; Hannington et al., 1995), this is an “active” mineralization process mediated by large organisms such as polychaete worms. These organisms secrete mucous layers, which, through adsorption or complexation with soluble species in the

organic matrix, are subsequently replaced and mineralized to form sulfide precipitation layers. For the laminate structure, as discussed in other hydrothermal fields (e.g., Lilliput, Dekov et al., 2010; PACMANUS, Zeng et al., 2012), we propose that this is a “passive” mineralization process associated with biofilm-forming microbial mats. The metabolic products of these mats provide nucleation surfaces for hydrothermal minerals and promote their precipitation, forming amorphous silica and sulfide mineral layers covering the bacterial layer. The globular pyrite is generally considered to be characteristic of biological sulfate reduction products (Piercey, 2015). Although the globular pyrite having lower $\delta^{34}\text{S}$ values than abiotic pyrite, exhibits much less sulfur isotope fractionation compared to other biogenically reduced pyrites (e.g. Nozaki et al., 2020; Ding et al., 2021). We suggest that this is a microbial assimilatory sulfate reduction process rather than dissimilatory sulfate reduction (Canfield, 2001), which results in only moderate sulfur isotope fractionation. Moreover, the microbial biofilm may be key to the aggregation of pyrite into a regular globular shape.

Whether it is macrobial or microbial mineralization, the selective adsorption of specific elements is a common feature of biogenic mineralization in this field, particularly in the case of

TABLE 3 *In-situ* sulfur isotopic compositions of sulfide biogenic/abiotic minerals in the Tongguan hydrothermal field.

Mineral	$\delta^{34}\text{S}$ (‰)	1σ	Mineral	$\delta^{34}\text{S}$ (‰)	1σ	Mineral	$\delta^{34}\text{S}$ (‰)	1σ	
Biogenic Minerals									
<i>Str. Py</i>	2.7	0.4	<i>Gl. Py</i>	2.3	0.6	<i>Onc. Ccp</i>	3.6	0.5	
	2.9	0.4		2.7	0.6		3.4	0.7	
	3.5	0.5		2.4	0.5		3.2	0.6	
	2	0.4		2.6	0.5		2.6	0.4	
<i>Onc. Py</i>	3.4	0.6		2.3	0.4		3.2	0.6	
	3.7	0.7		1.6	0.5		2.6	0.8	
<i>Tu. Py</i>	2.8	0.5		2	0.4				
	3.3	0.6		2.3	0.4				
	4.1	0.5		2.1	0.4				
<i>Gl. Py</i>	1.3	0.5		1.6	0.6				
	2.0	0.6		2.8	0.6				
Abiotic Minerals									
<i>Ab. Ccp</i>	4.2	0.4	<i>Ab. Py</i>	4.5	0.5				
	4.2	0.7		4.3	0.4				
				4.5	0.7				
				5.3	0.3				
				5.3	0.3				
				4.0	0.6				
				4.4	0.5				

Tu. Py, pyrite on tube wall, Str. Py, Quasi-stromatolite Pyrite, Onc. Py, Quasi-oncolite Pyrite, Onc. Ccp, Quasi-oncolite Chalcopyrite, Gl. Py, Globular Pyrite, Ab. Py, Abiotic pyrite, Ab. Ccp, Abiotic chalcopyrite.

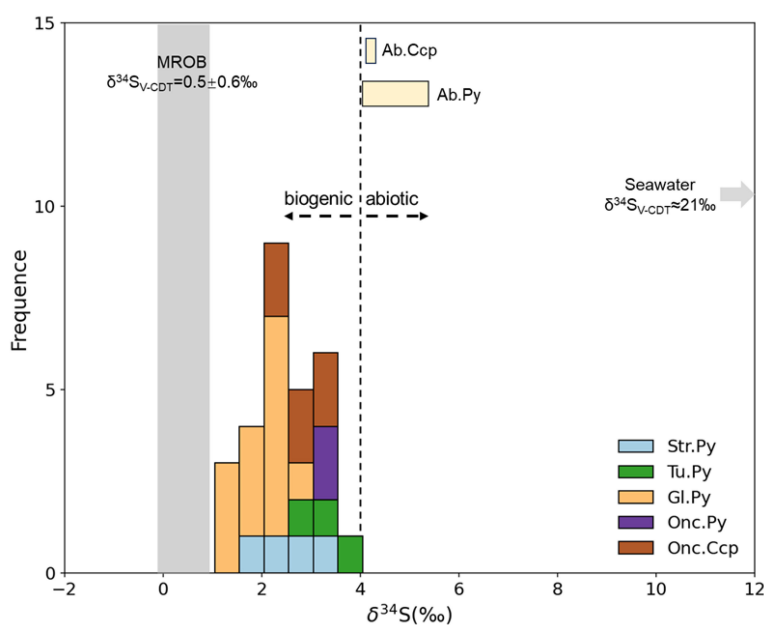


FIGURE 9 Frequency distribution of $\delta^{34}\text{S}$ values for different sulfides from the Tongguan hydrothermal field. Tu. Py, pyrite on tube wall, Str. Py, Quasi-stromatolite Pyrite, Onc. Py, Quasi-oncolite Pyrite, Onc. Ccp, Quasi-oncolite Chalcopyrite, Gl. Py, Globular Pyrite, Ab. Py, Abiotic pyrite, Ab. Ccp, Abiotic chalcopyrite. Data sources: Seawater (Rees et al., 1978), sulfides in MORB (Sakai et al., 1984).

pyrite. This widespread mediation by biofilms has led to increased concentrations of elements such as Mn and Pb. We speculate that the potential hydrothermal biotic mediation process selectively

precipitates specific elements, which may contribute to the enrichment of certain metals in certain submarine hydrothermal base metal sulfide deposits.

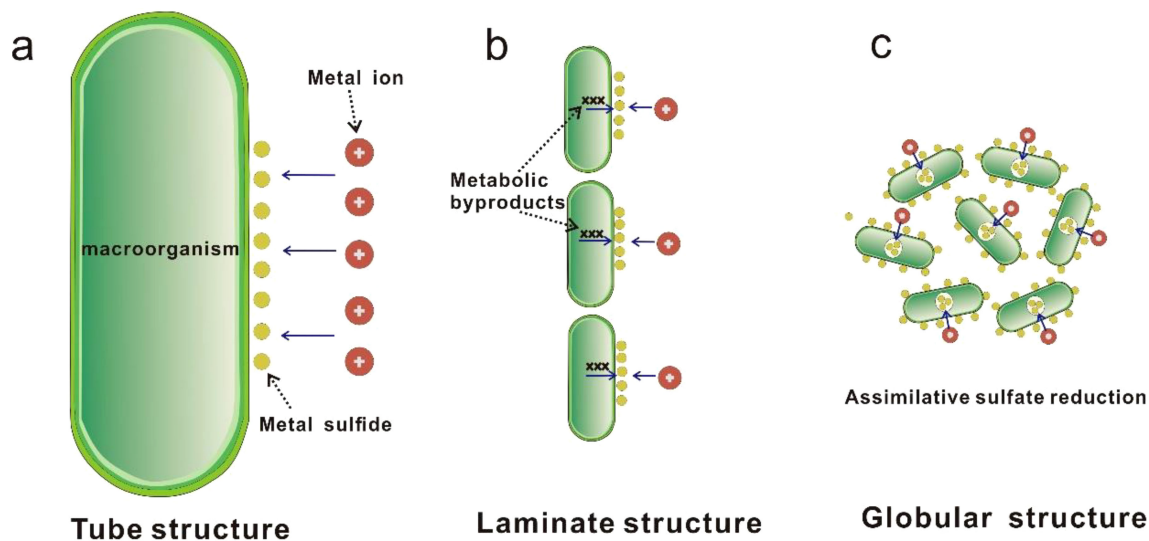


FIGURE 10 Schematic illustration of three types of biomineralization in the studied Tongguan sulfide samples (modified after Park and Damien, 2021). (a) The "active" mediation by macro-organisms, represented by polychaete worms, which involves the secretion of a mucous layer to capture metals from environment and subsequently precipitate them in the form of sulfides. (b) The "active" mediation by micro-organisms, where microorganism metabolic byproducts excreted by microorganisms provide nucleation surfaces for hydrothermal minerals and promote their precipitation, forming a laminate structure along the surface of a microbial mat composed of numerous microorganisms. (c) Formation of pyrite spherules through mixing of biogenic pyrite derived from biotic assimilative sulfate reduction reactions and adsorption of biofilms.

6 Conclusions

This study investigated chimney sample from the volcanic-hosted Tongguan hydrothermal field on the SMAR and presented several lines of evidence for Biogeochemical mineralization. Four types of biogenic structures were proposed: macrobiotic tube structure, microbial mat-related stromatolite- and oncolite-like structures, and globular structure. The pyrite within these biogenic structures exhibited selective enrichment of elements such as Mn, Pb, and Cu compared to abiogenic pyrite. *In-situ* sulfur isotope studies revealed that biogenic minerals possess lower $\delta^{34}\text{S}$ values than abiogenic minerals.

Both macro-organisms and microorganisms are involved in the mineralization process, facilitating mineral precipitation through different mechanisms. Three mechanisms by which hydrothermal organisms may facilitate mineral precipitation were identified: an “active” mineralization process mediated by large organisms like polychaete worms, a “passive” mineralization process associated with microbial mats, and a microbial assimilatory sulfate reduction process. Macrobiotic mineralization can coexist with microbial mineralization, which also needs attention.

Data availability statement

The original contributions presented in the study are included in the article/[Supplementary Material](#). Further inquiries can be directed to the corresponding authors.

Author contributions

BL: Data curation, Formal Analysis, Investigation, Methodology, Writing – original draft. XS: Funding acquisition, Project administration, Resources, Supervision, Writing – review & editing. CL: Funding acquisition, Project administration, Resources, Writing – review & editing. SW: Methodology, Writing – review & editing. JY: Writing – review & editing. QY: Funding acquisition, Writing – review & editing. YD: Methodology, Writing – review & editing. XF: Methodology, Writing – review & editing.

Funding

The author(s) declare that financial support was received for the research and/or publication of this article. This paper is financially supported by the National Key Research and Development Program of China (No.2024YFC2815200 and No.2022YFC2803800), the China Ocean Mineral Resources R&D Association project (Grant No. DY135-S2-2-06), Laoshan Laboratory (Grant Nos. LSKJ202203601, LSKJ202204103) and Taishan Scholar Program of Shandong province.

Acknowledgments

We thank all the crews and scientists of the 33rd and 83rd ocean expedition of China.

Conflict of interest

The authors declare that the research was conducted in the absence of any commercial or financial relationships that could be construed as a potential conflict of interest.

Generative AI statement

The author(s) declare that no Generative AI was used in the creation of this manuscript.

Publisher's note

All claims expressed in this article are solely those of the authors and do not necessarily represent those of their affiliated organizations, or those of the publisher, the editors and the reviewers. Any product that may be evaluated in this article, or claim that may be made by its manufacturer, is not guaranteed or endorsed by the publisher.

Supplementary material

The Supplementary Material for this article can be found online at: <https://www.frontiersin.org/articles/10.3389/fmars.2025.1562763/full#supplementary-material>

SUPPLEMENTARY TABLE 1

Chemical compositions of pyrite on tube wall as determined by EPMA analysis. Tu. Py, pyrite on tube worm wall. nd, non detected.

SUPPLEMENTARY TABLE 2

Chemical compositions of laminate pyrite and chalcopyrite as determined by EPMA analysis. La. Py, Laminate Pyrite; La. Ccp, Laminate Chalcopyrite. nd, non detected.

SUPPLEMENTARY TABLE 3

Chemical compositions of quasi-oncolite pyrite and chalcopyrite as determined by EPMA analysis. Qu. Py, Quasi-oncolite Pyrite; Qu. Ccp, Quasi-oncolite Chalcopyrite. nd, non detected.

SUPPLEMENTARY TABLE 4

Chemical compositions of framboidal pyrite as determined by EPMA analysis. Fr. Py, Framboidal Pyrite. nd, non detected.

SUPPLEMENTARY TABLE 5

Chemical compositions of abiogenic pyrite in the vicinity of biogenic minerals as determined by EPMA analysis. Ab. Py, Abiogenic pyrite. nd, non detected.

SUPPLEMENTARY TABLE 6

Chemical compositions of abiogenic chalcopyrite in the vicinity of biogenic minerals as determined by EPMA analysis Ab. Ccp, Abiogenic chalcopyrite. nd, non detected.

References

- Amend, J. P., McCollom, T. M., Hentscher, M., and Bach, W. (2011). Catabolic and anabolic energy for chemolithoautotrophs in deep-sea hydrothermal systems hosted in different rock types. *Geochim. Cosmochim. Acta* 75, 5736–5748. doi: 10.1016/j.gca.2011.07.041
- Black, M. B., Trivedi, A., Maas, P. A. Y., and Vrijenhoek, R. C. (1998). Population genetics and biogeography of vestimentiferan tube worms. *Deep-Sea Res.* 45, 365–382. doi: 10.1016/S0967-0645(97)00076-3
- Bright, M., Gollner, S., de Oliveira, A. L., Espada-Hinojosa, S., Fulford, A., Hughes, IV, et al. (2024). Animal life in the shallow seafloor crust at deep-sea hydrothermal vents. *Nat. Commun.* 15, 8466. doi: 10.1038/s41467-024-52631-9
- Canfield, D. E. (2001). Biogeochemistry of sulfur isotopes. *Rev. Mineralogy Geochemistry*. 43, 607–636. doi: 10.2138/gsrmg.43.1.607
- Cavanaugh, C. M., Gardiner, S. L., Jones, M. L., Jannasch, H. W., and Waterbury, J. B. (1981). Prokaryotic cells in the hydrothermal vent tube worm *Riftia pachyptila* Jones: possible chemoautotrophic symbionts. *Science* 213, 340–342. doi: 10.1126/science.213.4505.340
- Cook, T. L., and Stakes, D. S. (1995). Biogeological mineralization in deep-sea hydrothermal deposits. *Science* 267 (5206), 1975–1979. doi: 10.1126/science.267.5206.1975
- Corliss, J. B., Dymond, J., Gordon, L. I., Edmond, J. M., von Herzen, R. P., Ballard, R. D., et al. (1979). Submarine thermal springs on the galapagos rift. *Science* 203, 1073–1083. doi: 10.1126/science.203.4385.1073
- Dekov, V. M., Petersen, S., Garbe-Schönberg, C.-D., Kamenov, G. D., Perner, M., Kuzmann, E., et al. (2010). Fe–si-oxhydroxide deposits at a slow-spreading centre with thickened oceanic crust: The lilliput hydrothermal field (9°33'S, mid-atlantic ridge). *Chem. Geology* 278 (3–4), 186–200.
- Dick, G. J. (2019). The microbiomes of deep-sea hydrothermal vents: distributed globally, shaped locally. *Nat. Rev. Microbiol.* 17, 271–283. doi: 10.1038/s41579-019-0160-2
- Ding, T., Tao, C., Dias, Á.A., Liang, J., Chen, J., Wu, B., et al. (2021). Sulfur isotopic compositions of sulfides along the Southwest Indian Ridge: implications for mineralization in ultramafic rocks. *Miner Deposita* 56, 991–1006. doi: 10.1007/s00126-020-01025-0
- Duverger, A., Bernard, S., Viennet, J.-C., Miot, J., and Busigny, V. (2021). Formation of pyrite spherules from mixtures of biogenic FeS and organic compounds during experimental diagenesis. *Geochemistry Geophysics Geosystems* 22, e2021GC010056. doi: 10.1029/2021GC010056
- Fouquet, Y., Cambon, P., Etoubleau, J., Charlou, J. L., Ondreas, H., Barriga, F. J. A. S., et al. (2013). Geodiversity of hydrothermal processes along the mid-atlantic ridge and ultramafic-hosted mineralization: A new type of oceanic Cu-Zn-Co-Au volcanogenic massive sulfide deposit. *Geophysical Monograph Ser.* 188, 321–367. doi: 10.1029/2008GM000746
- Früh-Green, G., Kelley, D., Lilley, M., Cannat, M., Chavagnac, V., Baross, J., et al. (2022). Diversity of magmatism, hydrothermal processes and microbial interactions at mid-ocean ridges. *Nat. Rev. Earth Environ.* 3, 852–871. doi: 10.1038/s43017-022-00364-y
- Georgieva, M. N., Little, C. T. S., Bailey, R. J., Ball, A. D., and Glover, A. G. (2018). Microbial-tubeworm associations in a 440 million year old hydrothermal vent community. *Proc. Biol. Sci.* 285, 20182004. doi: 10.1098/rspb.2018.2004
- Grotzinger, J., and Al-Rawahi, Z. (2014). Depositional facies and platform architecture of microbialite-dominated carbonate reservoirs, Ediacaran–Cambrian Ara Group, Sultanate of Oman. *AAPG Bull.* 98, 1453–1494. doi: 10.1306/02271412063
- Hannington, M. D., Jonasson, I. R., Herzig, P. M., and Petersen, S. (1995). “Physical and chemical processes of seafloor mineralization at mid-ocean ridges,” in *Seafloor Hydrothermal Systems: Physical, Chemical, Biological, and Geological Interactions*. Eds. S. E. Humphris, R. A. Zierenberg, L. S. Mullineaux and R. E. Thomson (Washington, DC: American Geophysical Union), 115–157.
- Hannington, M. D., and Scott, S. D. (1988). Mineralogy and geochemistry of a hydrothermal silica-sulfide-sulfate spire in the caldera of Axial Seamount, Juan De Fuca Ridge. *Can. Mineralogist* 26, 603–625.
- Haymon, R. M. (1983). Growth history of black smoker hydrothermal chimneys. *Nature* 301, 695–698. doi: 10.1038/301695a0
- Hohl, S. V., and Viehmann, S. (2021). Stromatolites as geochemical archives to reconstruct microbial habitats through deep time: Potential and pitfalls of novel radiogenic and stable isotope systems. *Earth-Science Rev.* 218, 103683. doi: 10.1016/j.earscirev.2021.103683
- Humphris, S. E., Zierenberg, R. A., Mullineaux, L. S., and Thomson, R. E. Eds. (1995). *Seafloor Hydrothermal Systems: Physical, Chemical, Biological, and Geological Interactions*. In: *Geophysical Monograph*. (Washington, DC: AGU). doi: 10.1029/GM091
- Jiang, X. D., Sun, X. M., Guan, Y., Gong, J. L., Lu, Y., Lu, R. F., et al. (2017). Biomineralisation of the ferromanganese crusts in the Western Pacific Ocean. *J. Asian Earth Sci.* 136, 58–67. doi: 10.1016/j.jseas.2017.01.025
- Jonasson, I. R., and Walker, D. A. (1987). Micro-organisms and their debris as substrates for metal sulfide nucleation and accumulation in some mid-ocean ridge deposits (abstract) EOS, Trans. AGU 68, 1546. doi: 10.1029/93JB02871
- Juniper, S. K., and Fouquet, Y. (1988). Filamentous iron-silica deposits from modern and ancient hydrothermal sites. *Can. Mineral.* 26, 859–869.
- Juniper, S. K., Jonasson, I. R., Tunncliffe, V., and Southward, A. J. (1992). Influence of a tube-building polychaete on hydrothermal chimney mineralization. *Geology* 20, 895–898.
- Juniper, S. K., Thompson, J. A. J., and Calvert, S. E. (1986). Accumulation of minerals and trace elements in biogenic mucus at hydrothermal vents, Deep Sea Research Part A. *Oceanographic Res. Papers* 33, 339–347. doi: 10.1016/0198-0149(86)90095-6
- Keith, M., Häckel, F., Haase, K. M., Schwarz-Schampera, U., and Klemm, R. (2016). Trace element systematics of pyrite from submarine hydrothermal vents. *Ore Geology Rev.* 72, 728–745. doi: 10.1016/j.oregeorev.2015.07.012
- Koski, R. A., Jonasson, I. R., Kadko, D. C., Smith, V. K., and Wong, F. L. (1994). Compositions, growth mechanisms, and temporal relations of hydrothermal sulfide-sulfate-silica chimneys at the northern Cleft segment, Juan de Fuca Ridge. *J. Geophys. Res.* 99, 4813. doi: 10.1029/93JB02871
- Little, C. T. S., Herrington, R. J., Maslennikov, V. V., Morris, N. J., and Zaykov, V. V. (1997). Silurian hydrothermal-vent community from the southern Urals, Russia. *Nature* 385, 146–148. doi: 10.1038/385146a0
- Maslennikov, V. V., Maslennikova, S. P., Large, R. R., and Danyushevsky, L. V. (2009). Study of trace element zonation in vent chimneys from the silurian yaman-kasy volcanic-hosted massive sulfide deposit (Southern urals, Russia) using laser ablation-inductively coupled plasma mass spectrometry (LA-ICPMS). *Economic Geology*. 104, 1111–1141. doi: 10.2113/gsecongeo.104.8.1111
- Nozaki, T., Nagase, T., Ushikubo, T., Shimizu, K., Ishibashi, J.-i., and the D/V Chikyū Expedition 909 Scientists (2020). Microbial sulfate reduction plays an important role at the initial stage of seafloor sulfide mineralization. *Geology* 49, 222–227. doi: 10.1130/GEOL.S.12964949.v1
- Nutman, A. P., Bennett, V. C., Friend, C. R. L., Kranendonk, M. J. V., and Chivas, A. R. (2016). Rapid emergence of life shown by discovery of 3,700-million-year-old microbial structures. *Nature* 537, 535–538. doi: 10.1038/nature19355
- Ohfuji, H., and Rickard, D. (2005). Experimental syntheses of framboids—a review. *Earth-Science Rev.* 71 (3–4), 147–170.
- Park, Y., and Damien, F. (2021). Diversity of microbial metal sulfide biomineralization. *ChemPlusChem* 87, e202100457. doi: 10.1002/cplu.202100457
- Pedersen, R. B., Rapp, H. T., Thorseth, I. H., Lilley, M. D., Barriga, F. J. A. S., Baumberg, T., et al. (2010). Discovery of a black smoker vent field and vent fauna at the Arctic Mid-Ocean Ridge. *Nat. Commun.* 1, 126. doi: 10.1038/ncomms1124
- Piercey, S. J. (2015). A semipermeable interface model for the genesis of seafloor replacement-type volcanogenic massive sulfide (VMS) deposits. *Economic Geology*. 110, 1655–1660. doi: 10.2113/econgeo.110.7.1655
- Piercey, S. J., Squires, G., and Brace, T. (2018). Geology and lithochemistry of hydrothermal mudstones from the upper block near the Duck Pond volcanogenic massive sulfide (VMS) deposit, Newfoundland, Canada: evidence for low-temperature venting into oxygenated mid-Cambrian seawater. *Miner Deposita* 53, 1167–1191. doi: 10.1007/s00126-018-0795-3
- Rees, C. E., Jenkins, W. J., and Jan, M. (1978). The sulphur isotopic composition of ocean water sulphate. *Geochimica Cosmochimica Acta* 42 (4), 377–381.
- Reid, R. P., Visscher, P. T., Decho, A. W., Stolz, J. F., Bebout, B. M., Dupraz, C., et al. (2000). The role of microbes in accretion, lamination and early lithification of modern marine stromatolites. *Nature* 406, 989–992. doi: 10.1038/35023158
- Reysenbach, A., Banta, A. B., Boone, D. R., Cary, S. C., and Luther, G. W. (2000). Microbial essentials at hydrothermal vents. *Nature* 404, 835. doi: 10.1038/35009029
- Sakai, H., Marais, D. J. D., Ueda, A., and Moore, J. G. (1984). Concentrations and isotope ratios of carbon, nitrogen and sulfur in ocean-floor basalts. *Geochimica Cosmochimica Acta* 48 (12), 2433–2441.
- Sawlowicz, Z. (1993). Pyrite framboids and their development: a new conceptual mechanism. *Geol Rundsch* 82, 148–156. doi: 10.1007/BF00563277
- Schrenk, M. O., Kelley, D. S., Bolton, S. A., and Baross, J. A. (2004). Low archaeal diversity linked to seafloor geochemical processes at the Lost City hydrothermal field, Mid-Atlantic Ridge. *Environ. Microbiol.* 6, 1086–1095. doi: 10.1111/j.1462-2920.2004.00650.x
- Sievert Stefan, M., and Vetricani, C. (2012). Chemoautotrophy at deep-sea vents: past, present, and future. *Oceanography* 25, 218–233.
- Sim, M. S., Bosak, T., and Ono, S. (2011). Large sulfur isotope fractionation does not require disproportionation. *Science* 333, 74–77. doi: 10.1126/science.1205103
- Truong, C., Bernard, S., Gorlas, A., and Guyot, F. (2024). Abiotic syntheses of pyrite: clues to assess the biogenicity of pyrite spherules. *Geochem. Persp. Lett.* 32, 27–33. doi: 10.7185/geochemlet.2438

- Wacey, D., Kilburn, M. R., Saunders, M., Cliff, J. B., Kong, C., Liu, A. G., et al. (2015). Uncovering framboidal pyrite biogenicity using nano-scale CNorg mapping. *Geology* 43 (1), 27–30. doi: 10.1130/G36048.1
- Wang, S., Li, C., Li, B., Dang, Y., Ye, J., Zhu, Z., et al. (2022). Constraints on fluid evolution and growth processes of black smoker chimneys by pyrite geochemistry: A case study of the Tongguan hydrothermal field, South Mid-Atlantic Ridge. *Ore Geology Rev.* 140, 104410. doi: 10.1016/j.oregeorev.2021.104410
- Wang, X., and Müller, W. E. G. (2009). Marine biominerals: perspectives and challenges for polymetallic nodules and crusts. *Trends Biotechnol.* 27, 375–383. doi: 10.1016/j.tibtech.2009.03.004
- Weiss, M. P. (1969). Oncolites, paleoecology, and laramide tectonics, central Utah. *AAPG Bulletin*. 53, 1105–1120. doi: 10.1306/5D25C81F-16C1-11D7-8645000102C1865D
- Winn, C., Karl, D., and Massoth, G. (1986). Microorganisms in deep-sea hydrothermal plumes. *Nature* 320, 744–746. doi: 10.1038/320744a0
- Zeng, Z., Ouyang, H., Yin, X., Chen, S., Wang, X., and Wu, L. (2012). Formation of Fe–Si–Mn oxyhydroxides at the PACMANUS hydrothermal field, Eastern Manus Basin: Mineralogical and geochemical evidence. *J. Asian Earth Sci.* 60, 130–146. doi: 10.1016/j.jseaes.2012.08.009
- Zhao, J., Zhang, G. H., Wu, G., Lu, B., Pulyaeva, I. A., Zhang, H., et al. (2014). Biomineralization of organic matter in cobalt-rich crusts from the Marcus-Wake Seamounts of the western Pacific Ocean. *Acta Oceanologica Sin.* 33, 67–74. doi: 10.1007/s13131-014-0552-0
- Zierenberg, R. A., and Schiffman, P. (1990). Microbial control of silver mineralization at a sea-floor hydrothermal site on the northern Gorda Ridge. *Nature* 348, 155–157. doi: 10.1038/348155a0

Appendix A. Supplementary data

Chemical compositions of abiotic and biogenic pyrite and chalcopyrite in the studied Tongguan samples as determined by EPMA analysis are given in [Supplementary Tables 1-6](#).